01 Sep 2012

Spectroscopy and Dynamics of the Predissociated, Quasi-Linear S_2 State of Chlorocarbene

Chong Tao

Craig A. Richmond

Calvin Mukarakate

Scott H. Kable

et. al. For a complete list of authors, see https://scholarsmine.mst.edu/chem_facwork/360

Recommended Citation

C. Tao et al., "Spectroscopy and Dynamics of the Predissociated, Quasi-Linear S_2 State of Chlorocarbene," *Journal of Chemical Physics*, vol. 137, no. 10, American Institute of Physics (AIP), Sep 2012.
The definitive version is available at https://doi.org/10.1063/1.4748972

Spectroscopy and dynamics of the predissociated, quasi-linear S_2 state of chlorocarbene

Chong Tao,[1] Craig A. Richmond,[2] Calvin Mukarakate,[1] Scott H. Kable,[2] George B. Bacskay,[2,a)] Eric C. Brown,[3] Richard Dawes,[4,a)] Phalgun Lolur,[4] and Scott A. Reid[1,a)]

[1]*Department of Chemistry, Marquette University, Milwaukee, Wisconsin 53201-1881, USA*
[2]*School of Chemistry, The University of Sydney, NSW 2006, Australia*
[3]*Department of Chemistry, University of Loyola-Chicago, Chicago, Illinois 60660, USA*
[4]*Department of Chemistry, Missouri University of Science and Technology, Rolla, Missouri 65409, USA*

(Received 5 July 2012; accepted 15 August 2012; published online 10 September 2012)

In this work, we report on the spectroscopy and dynamics of the quasi-linear S_2 state of chlorocarbene, CHCl, and its deuterated isotopologue using optical-optical double resonance (OODR) spectroscopy through selected rovibronic levels of the S_1 state. This study, which represents the first observation of the S_2 state in CHCl, builds upon our recent examination of the corresponding state in CHF, where pronounced mode specificity was observed in the dynamics, with predissociation rates larger for levels containing bending excitation. In the present work, a total of 14 S_2 state vibrational levels with angular momentum $\ell = 1$ were observed for CHCl, and 34 levels for CDCl. The range of ℓ in this case was restricted by the pronounced Renner-Teller effect in the low-lying S_1 levels, which severely reduces the fluorescence lifetime for levels with $K_a > 0$. Nonetheless, by exploiting different intermediate S_1 levels, we observed progressions involving all three fundamental vibrations. For levels with long predissociation lifetimes, rotational constants were determined by measuring spectra through different intermediate J levels of the S_1 state. Plots of the predissociation linewidth (lifetime) vs. energy for various S_2 levels show an abrupt onset, which lies near the calculated threshold for elimination to form $C(^3P) + HCl$ on the triplet surface. Our experimental results are compared with a series of high level *ab initio* calculations, which included the use of a dynamically weighted full-valence CASSCF procedure, focusing maximum weight on the state of interest (the singlet and triplet states were computed separately). This was used as the reference for subsequent Davidson-corrected MRCI(+Q) calculations. These calculations reveal the presence of multiple conical intersections in the singlet manifold. © *2012 American Institute of Physics*. [http://dx.doi.org/10.1063/1.4748972]

I. INTRODUCTION

Carbenes represent one of the important classes of reactive chemical intermediates.[1,2] Much of the interest in carbenes stems from the electronic structure of the divalent carbon, which gives rise to nearly isoenergetic singlet and triplet configurations that exhibit distinct patterns of chemical reactivity. Thus, much experimental and theoretical effort has been invested in the study of the singlet-triplet gap and intersystem crossing of carbenes. Recently, our group reported spectroscopic studies of chlorocarbene (CHCl) that represented the first rotationally resolved spectrum of singlet-triplet transitions in a carbene.[3,4] In addition to providing a spectroscopically precise value for the singlet-triplet gap that was within several cm^{-1} (~0.01 kcal/mol) of recent high level *ab initio* predictions, our experiments showed a pronounced vibrational state dependence of the triplet spin-spin coupling constant, reflecting interactions with nearby singlet levels.[4] This provided a sensitive probe of the spin-orbit coupling, and our derived value for the electronic spin-orbit coupling matrix element was in excellent agreement with theoretical predictions.

The halocarbenes are the smallest carbenes with singlet ground states, and, being tractable to high level *ab initio* theory, have served as benchmark systems for understanding the properties of singlet carbenes.[1] Over the past several decades, the low lying (S_0, T_1, S_1) electronic states of the halocarbenes CXY (X = H, F, Cl, Br, I; Y = F, Cl, Br, I) have been extensively studied.[1] Much less is known, however, about the higher lying excited states. In the prototypical carbene, methylene (CH_2), a weak broken progression observed by Herzberg and Johns was assigned to the $\tilde{a}^1A_1 - \tilde{c}^1B_1$ system,[5] the equivalent of the S_0-S_2 system in carbenes with singlet ground states. This assignment has been recently confirmed by Sears and co-workers, who used optical-optical double resonance (OODR) methods to obtain rotationally resolved spectra of bands near and above the onset of predissociation.[6,7] We observed the predissociated, quasi-linear S_2 state of CHF and CDF using similar methods,[8] and recently reported detailed studies of the spectroscopy and dynamics.[9,10] All observed S_2 bands are broadened by dissociation, with larger widths observed for pure bending levels.[9] A 27-state dynamically weighted full-valence CASSCF calculation was performed with maximal weight focused on the S_2 state, which was then used as a reference for Davidson-corrected multireference configuration interaction calculations MRCI(+Q) of the three lowest A′ and

a)Authors to whom correspondence should be addressed. Electronic addresses: bacskay@chem.usyd.edu.au, dawesr@mst.edu, and scott.reid@mu.edu.

two lowest A″ states. These revealed the presence of multiple conical intersections (CI) in the singlet manifold, the most important of these involved the repulsive S_3 state, which conically intersects with S_2 and S_0 at linearity.[9]

Here we turn our attention to the heavier analogue, chlorocarbene (CHCl), with the goal of examining the influence of spin-orbit coupling on the dynamics of the S_2 state. Recently, Dagdigian and co-workers examined the photodissociation dynamics of a number of triatomic halocarbenes, including CHCl, at wavelengths of 248 and 193 nm.[11–15] In the case of CHCl, the diatomic product of the higher lying radical channel (forming $CH(^2\Pi) + Cl$) was detected via Laser Induced Fluorescence (LIF), following excitation of the parent carbene at 193 nm.[15] The CCl product of the lowest radical channel (forming $CCl(^2\Pi) + H$) could not be detected due to the large background of this radical in the beam. The $CH(^2\Pi)$ fragment displayed only modest levels of rotational and vibrational excitation; however, a marked propensity for formation of the A″ Λ-doublets was observed, which was taken to indicate that dissociation occurred from a non-linear excited state. In this case the identity of the parent state accessed at 193 nm was not clear; however, it was suggested by analogy with CCl_2 that a Rydberg state was being populated.[15]

The participation of carbenes as intermediates in the reactions of $C(^3P,^1D)$ with small molecules such as HCl has previously been postulated. In studies of the $C(^3P,^1D) + HCl$ reactions, Reisler and co-workers invoked the participation of intermediate singlet and triplet carbene states,[16–18] which were presumably accessed following insertion into the hydrogen halide bond. Guadagnini and Schatz reported quasiclassical trajectory studies of the $C(^3P) + HCl$ and $C(^3P) + H_2$ reactions,[19] which confirmed the predominance of an insertion mechanism, and identified an unusual insertion pathway occurring from nearly collinear geometries. They found that the majority of insertion events were unreactive and, except at low collision energies, the $CH(^2\Pi) + Cl$ channel was dominant.

In this work, we report the first studies of the S_2 state of the chlorocarbenes $CH^{35}Cl$ and $CD^{35}Cl$. The focus of this paper is on the spectroscopy and dynamics of the S_2 state. We report on the homogeneous linewidths in this system and their dependence on energy, which gives insight into the possible photochemical product(s). The outline of the paper is as follows: Sec. II describes the experimental and theoretical methodology, Sec. III summarizes our findings and provides a discussion of those findings in the light of prior experimental and theoretical studies, and Sec. IV contains a summary and conclusions.

II. EXPERIMENTAL AND THEORETICAL METHODS

The apparatus and approach used in this work is similar to that of previous studies.[3,4,8–10,20] Briefly, CHCl (CDCl) was produced using a pulsed discharge nozzle through a ∼1%–2% mixture of CH_2Cl_2 (CD_2Cl_2) in high purity He. Specific rotational transitions in various bands of the $S_0 \rightarrow S_1$ system[21,22] were excited by a tunable Nd:YAG pumped dye laser (Continuum P7010/Lambda Physik Scanmate 2E). Approximately 300–400 ns later, a pulse from a second Nd:YAG pumped dye laser (Spectra-Physics INDI/Syrah CobraStretch), counter-propagating with the first, either excited specific transitions in the $S_1 \rightarrow S_2$ system or stimulated emission from $S_1 \rightarrow S_0$. The latter process has been extensively studied in previous work from our lab,[3,4] and the S_0 level structure is well known. The decrease in fluorescence caused by the second (probe) laser was measured using a dual boxcar system (SRS 250), where a portion of the fluorescence decay was integrated before and after the second laser pulse. The ratio of the signal from each gate was taken on a shot by shot basis, and 10–20 shots were averaged at each step in wavelength. The wavelength of the pump laser was calibrated using the well-known $S_0 \rightarrow S_1$ spectroscopic constants,[21,22] calibrated to vacuum wavenumbers. The probe laser was calibrated using optogalvanic spectroscopy in a Fe:Ne hollow cathode lamp.

The S_1 levels used as intermediates in this work included for $CH^{35}Cl$ (0, *n*, 0) levels with $n = 2$-6, (0, *n*, 1) levels with $n = 4$–5, and (0, *n*, 2) levels with $n = 4$. For $CD^{35}Cl$, the following S_1 levels were used: (0, *n*, 0) levels with $n = 1$–7, (0, *n*, 1) levels with $n = 2$–7, and (1, *n*, 0) levels with $n = 0$–5. Access to transitions near the S_2 origin required longer probe wavelengths than were attainable with our dye laser system. Thus, a home-built Raman shifter, pressurized to ∼30 bars with H_2, was used to shift the dye laser fundamental into the near-infrared (NIR) spectral region, using the first Stokes transition. The dye laser was loosely focused into the shifter with a 0.5 m lens, and the output was optically filtered to remove the anti-Stokes and higher order Stokes lines and recollimated with a second lens. The shifter was placed immediately before the chamber entrance window to minimize losses of the NIR beam.

For calculations, the ground atomic states for hydrogen $H(^2S_g)$ and chlorine $Cl(^2P_u)$ were combined with the three lowest atomic states of carbon $C(^3P_g)$, $C(^1D_g)$, and $C(^1S_g)$ to form 27 singlet ($14\ ^1A' + 13\ ^1A''$) and 36 triplet ($18\ ^3A' + 18\ ^3A''$) molecular states in C_S symmetry. Calculations relating to any particular molecular state of interest were performed using a dynamically weighted full-valence CASSCF procedure, focusing maximum weight on the state of interest (the singlet and triplet states were computed separately).[23] This was used as the reference for subsequent Davidson-corrected MRCI(+Q) calculations. The MOLPRO code was used to perform all of the electronic structure calculations reported here.[24] To gain a qualitative understanding of the behavior of the low-lying states, a series of 1D cuts and 2D scans were plotted (see, e.g., Fig. 1 and Fig. S1–S3 in supplementary material).[25] The electronic structure of CHCl is similar to that of CHF, exhibiting numerous conical intersections (CI) between the low-lying states (Fig. 1). Complete basis set (CBS) extrapolation is a useful procedure to obtain highly accurate results, but extrapolation in the adiabatic representation can cause disruptions in the PES near a CI. Thus the data plotted in Fig. 1 and S1–S3 were computed using the aug-cc-pV(Q+d)Z basis only.

To compute accurate gaps between states we employed CBS extrapolations and also included corrections such as core-correlation, relativistic, and ZPE effects. The optimized geometries and harmonic frequencies were obtained for each

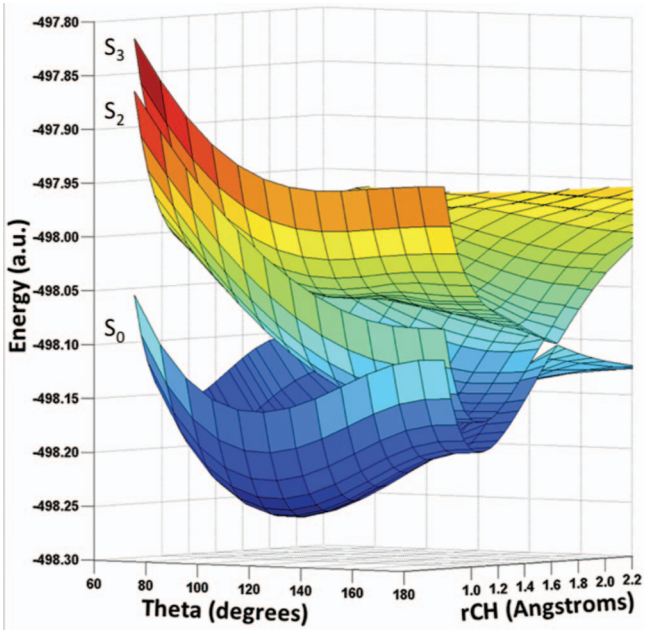

FIG. 1. 2D Plot of three lowest $^1A'$ states (S_0, S_2, and S_3, solid color) with C–Cl distance fixed (rCCl = 1.6 Å). S_3 is seen to cross S_2 and S_0 at $\theta = 180^\circ$, but the crossings are avoided at bent geometries.

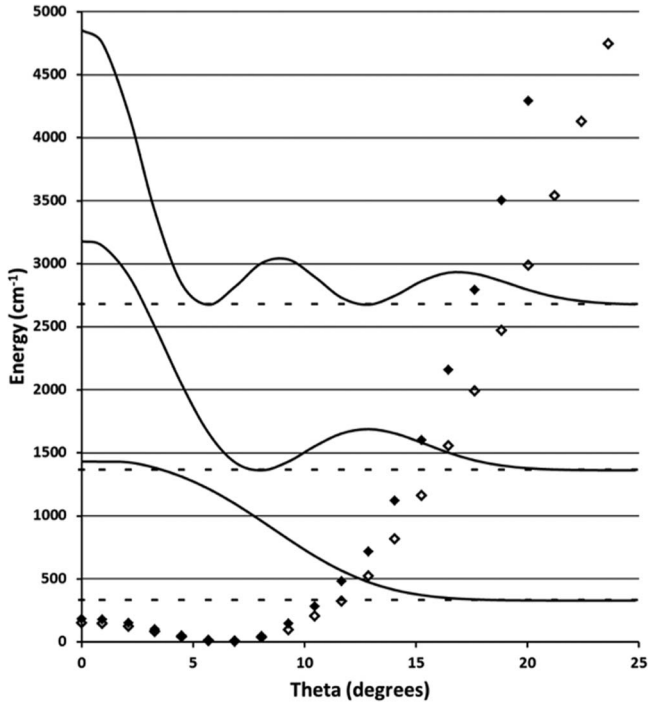

FIG. 2. Plots (points) of a 1D scan of the S_2 potential of CHCl in Jacobi coordinates. Filled symbols correspond to fixed C–H, C–Cl distances, open symbols are fully relaxed. The fully relaxed scan was used to solve the 1D bend Hamiltonian using a Legendre DVR.

of the S_0, S_1, S_2, and T_1 molecular states using a numerical procedure directly on the CBS extrapolated surface. At each point the dynamically weighted state-averaged CASSCF procedure was used followed by MRCI(+Q) calculations with the aug-cc-pV(T+d)Z and aug-cc-pV(Q+d)Z bases, extrapolated using the l^{-3} formula.[26] Only the valence electrons were correlated in the geometry optimizations and harmonic frequency calculations. Using the obtained geometries, energy gaps between the states were computed from MRCI(+Q) energies (with all electrons correlated) using the basis set series aug-cc-pwCVnZ (n = 3–5). The reference, correlation, and Davidson-correction contributions to the energies were separately extrapolated using an optimized power-law $E_{l_{\max}} = E_{CBS} + Al_{\max}^{-pow}$, where $l_{\max}$ is the cardinal number of the basis and *pow* is an optimized exponent.[27] Relativistic corrections were computed as differences from energies computed the same way except using the 8th order Douglas-Kroll-Hess Hamiltonian as implemented in MOLPRO.

Since the S_2 state is quasi-linear with the calculated minimum of the potential at $\theta_e = 166.3^\circ$, and the calculated barrier to linearity only ~145 cm^{-1}, much less than the Zero-Point Energy (ZPE), the harmonic approximation is a very poor description of the bend degree of freedom. A 1D scan of the potential was performed in Jacobi coordinates, relaxing the two stretching coordinates at each point (see Fig. 2). The scan was used to solve the 1D bend Hamiltonian using a Legendre DVR. The ZPE from the calculated (0, n^0, 0) [n = 0, 2, . . .] progression was used instead of the harmonic approximation for the bend coordinate. Also, the experimentally recorded progression (0, n^1, 0) [n = 3, 5, . . . , 17] was fit to the calculated progression for the purpose of extrapolating to the state origin.

III. RESULTS AND DISCUSSION

Following our previous study of CHF, where essentially all S_2 levels were homogeneously broadened,[8] we anticipated a similar situation for CHCl. Indeed, our initial survey revealed a number of broad features that were readily assigned to vibrational levels of the S_2 state (see Figs. 3 and 4 for examples). One important distinction between CHF and CHCl lies in the fact that all intermediate S_1 levels used for CHCl are above the barrier to linearity, where the only intense and unperturbed sub-band is that which terminates in $K_a = 0$.[21,22,28–31] The $K_a - l = \pm 1$ selection rule, where l is

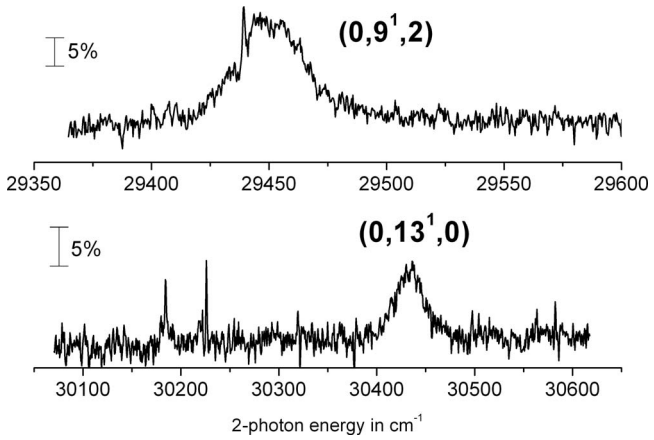

FIG. 3. Optical-optical double resonance (OODR) spectra of the S_2 state of $CH^{35}Cl$. The broad features represent upward transition to the S_2 state, while narrow features reflect downward (SEP) transitions to known vibrational levels of the S_0 state.

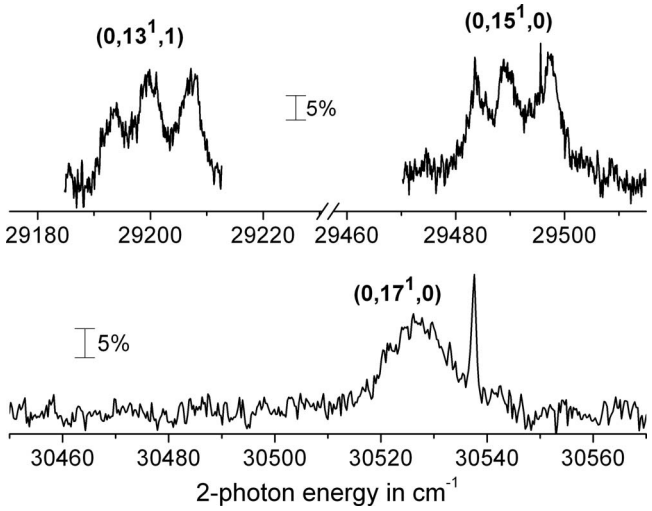

FIG. 4. Optical-optical double resonance (OODR) spectra of the S_2 state of $CD^{35}Cl$. The rotationally resolved spectra in the upper panel were obtained through an intermediate rovibrational level of the S_1 state with $J = 5$ and $K_a = 0$.

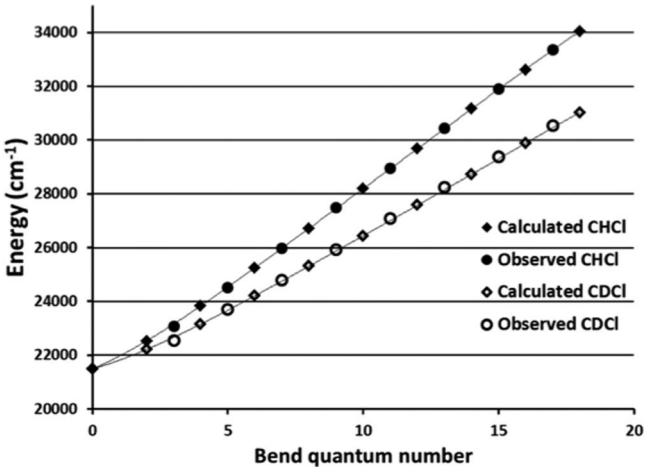

FIG. 5. Plots of a 5th-order polynomial fit to the calculated (0, n^0, 0) $n = 0$, 2, …, 18 even progressions matched up with the experimentally observed (0, n^1, 0) $n = 3, 5, \ldots, 17$ odd progressions for CHCl and CDCl.

the vibrational angular momentum quantum number for the bending mode in the quasi-linear S_2 state and K_a is the associated rotational quantum number of the bent molecule in the S_1 state, thus restricts $l = 1$; i.e., only odd vibrational levels in the S_2 state can be observed. However, by pumping different intermediate (S_1) levels in the progressions 2_0^n, $1_0^1 2_0^n$, and $2_0^n 3_0^1$,[21,22] a variety of S_2 levels were accessed. The isotope splittings in the S_0-S_1 bands are sufficient to afford clean excitation of one chlorine isotopologue,[21,22] and all of the spectra reported here are for the $CH(D)^{35}Cl$ isotopologue.

For most of the bands measured here, significant homogeneous broadening precluded a rotational analysis; however, for those weakly predissociated bands displaying rotational structure (see Fig. 4 for example), the observed rotational transitions were fit to a linear molecule rotational Hamiltonian using a nonlinear least squares routine to derive the band origin and effective rotational constant. Note that an additional selection rule governs transitions between each asymmetry doublet in the S_1 state with levels of different parity in the S_2 state, however, we do not resolve the asymmetry nor parity doublets in these experiments. Table I provides a listing of the observed band positions and constants for $CH^{35}Cl$ and $CD^{35}Cl$, sorted by progression.

Due to a poor Franck-Condon factor coupled with a lack of sensitivity, we were unable to observe the S_2 origin in this work. In the quasi-linear S_2 state, the harmonic approximation is a poor description of the bend degree of freedom; in fact, the very low barrier to linearity (calculated at 145 cm^{-1}) places CHCl close to the linear molecule limit. One dimensional (1D) scans of the bend coordinate are plotted in Figure 2 comparing fixed and relaxed r_{CCl} and r_{CH} bond distances. Levels computed using the relaxed curve are in much better agreement with the experimental progression. A 5th-order polynomial fit to the calculated (0, n^0, 0) [n = 0, 2, …, 18] even progression can be matched up with the experimentally observed (0, n^1, 0) [n = 3, 5, …, 17] odd progression with an RMS error of 33 cm^{-1} (Fig. 5). The fit for CDCl is slightly worse as the experimental (0, 3^1, 0) state in particular seems to be perturbed by interaction with other states. Obviously such interactions are not captured in the 1D calculation. Using this extrapolation of the experimental levels the origin of the S_2 state was placed at 21 491 cm^{-1} above the ground state compared with a calculated origin of 21 845 cm^{-1}. It is anticipated that future vibrational calculations using a coupled description of the S_0, S_1, S_2, and T_1 electronic states, and also accounting for the non-zero angular momentum will achieve better agreement and interpretation of the experimental data.

Further information on the S_2 term energy and vibrational structure comes from a fit of the observed energy levels to a linear molecule Dunham expansion of the form:[32]

$$G_0(\upsilon_1, \upsilon_2^\ell, \upsilon_3) = \sum_{i=1}^{3} \upsilon_i \omega_i^0 + \sum_{j \geq i, i=1}^{3} \upsilon_i \upsilon_j x_{ij}^0 + g_{22} \ell (\ell + 1). \quad (1)$$

As only levels with $l = 1$ were observed, g_{22} could not be determined and was set to zero in the fit. The fit parameters are listed in Table II. While the expression in Eq. (1) provides overall only a fair description of the observed energy levels, it nonetheless suggests an origin for the S_2 state similar to that determined from the procedure described above, and provides reasonable estimates of the vibrational frequencies in the S_2 state for both isotopolouges. Particularly striking is the pronounced increase in the C–H and C–Cl stretching frequencies relative to the lower-lying singlet states. For example, the C–Cl stretching frequency in $CH^{35}Cl$ increases from 812 cm^{-1} (S_0) to 926 cm^{-1} (S_1) to 1032 cm^{-1} (S_2), while the C–H stretching frequency increases from 2803 cm^{-1} (S_0) to 2980 cm^{-1} (S_1) to 3173 cm^{-1} (S_2). Similarly, for $CD^{35}Cl$ the C–Cl stretching frequency increases from 801 cm^{-1} (S_0) to 901 cm^{-1} (S_1) to 946 cm^{-1} (S_2), while the C–D stretching frequency increases from 2078 cm^{-1} (S_0) to 2230 cm^{-1} (S_1) to 2393 cm^{-1} (S_2).

Previous multireference calculations of the S_0, S_1, and T_1 states by Yu *et al.* employed only the aug-cc-pVTZ basis

TABLE I. Assignments, energies, rotational constants, and linewidths of all $CH^{35}Cl$ and $CD^{35}Cl$ S_2 state vibrational levels measured in this work.

	$CH^{35}Cl$			$CD^{35}Cl$		
Level	Term energy (cm^{-1})	B (cm^{-1})	Linewidth (cm^{-1})	Term energy (cm^{-1})	B (cm^{-1})	Linewidth (cm^{-1})
$(0,3^1,0)$	23076.8(5)	…	…	22559.1(5)	…	…
$(0,5^1,0)$	24519.4(5)	…	…	23705.4(1)	…	…
$(0,7^1,0)$	25987.5(3)	0.575(8)	…	24780.0(3)	0.534(9)	…
$(0,9^1,0)$	27480.5(2)	0.565(6)	1.9(5)	25928.9(9)	0.532(31)	1.4(4)
$(0,11^1,0)$	28964.0(1)	0.593(7)	7.9(27)	27086.6(4)	0.513(14)	1.35(9)
$(0,13^1,0)$	30433(2)	…	32(5)	28237.0(23)	0.527(54)	3.9(18)
$(0,15^1,0)$	31899(2)	…	20(5)	29391.5(26)	0.525(61)	5.6(24)
$(0,17^1,0)$	33356(2)	…	36(5)	30533(1)	…	10.9(15)
$(0,3^1,1)$	…	…	…	23548.8(2)	…	…
$(0,5^1,1)$	…	…	…	24618.7(2)	0.527(5)	…
$(0,7^1,1)$	…	…	…	25737.4(16)	0.510(51)	…
$(0,9^1,1)$	…	…	…	26786.7(2)	0.524(14)	1.5(3)
$(0,11^1,1)$	29952(2)	…	22(5)	28029.7(10)	0.517(47)	2.2(6)
$(0,13^1,1)$	31398(2)	…	24(3)	29177.2(2)	0.539(5)	4.8(3)
$(0,15^1,1)$	32887(3)	…	37(5)	…	…	…
$(0,7^1,2)$	…	…	…	26683.7(1)	0.522(9)	0.6(2)
$(0,9^1,2)$	29455(2)	…	25(3)	27816.0(3)	0.516(11)	1.8(7)
$(0,11^1,2)$	…	…	…	28967(1)	…	…
$(0,13^1,2)$	32380(3)	…	22(3)	30103.3(8)	0.542(25)	4.7(7)
$(0,15^1,2)$	…	…	…	31248(2)	…	23(3)
$(0,5^1,3)$	…	…	…	26518.1(1)	0.520(2)	0.5(2)
$(0,7^1,3)$	…	…	…	…	…	…
$(0,9^1,3)$	…	…	…	28751(2)	…	…
$(0,11^1,3)$	…	…	…	29883(1)	…	4.0(10)
$(0,13^1,3)$	…	…	…	31025(1)	…	8.6(10)
$(0,9^1,4)$	…	…	…	29668(1)	…	…
$(0,5^1,5)$	…	…	…	28321.3(1)	0.528(5)	2.7(5)
$(0,7^1,5)$	…	…	…	29468(2)	0.522(40)	4.3(12)
$(0,9^1,5)$	…	…	…	30601(1)	…	6.8(1)
$(0,11^1,5)$	…	…	…	31736(1)	…	13(5)
$(1,5^1,0)$				26071.3(5)	…	…
$(1,13^1,0)$	…	…	…	30689(1)	…	9.1(10)
$(1,15^1,0)$	…	…	…	31807(1)	…	11.4(26)
$(1,5^1,1)$	27705.6(5)	0.597(13)	2.6(7)	27044(1)	…	…
$(1,13^1,1)$	…	…	…	31610(1)	…	…
$(1,9^1,2)$	…	…	…	30216.0(1)	0.515(4)	…

TABLE II. $CH^{35}Cl/CD^{35}Cl$ S_2 vibrational parameters determined from the Dunham expansion fit.[a]

Parameter	$CH^{35}Cl$	$CD^{35}Cl$
T_{oo}	20 851(37)	20 884(21)
v_1[b]	3173(24)	2393(21)
ω_2	736(8)	555(5)
ω_3	1032(60)	946(8)
x_{11}	…	…
x_{12}	…	3.4(18)
x_{13}	…	−6(9)
x_{22}	0.0(4)	0.8(2)
x_{23}	−2(4)	−0.2(6)
x_{33}	−11(16)	−2.7(11)

[a]One standard error given in parenthesis with respect to least significant digit.
[b]Anharmonic frequency.

set (without core-correlation or other corrections) and were empirically scaled to achieve agreement with experimental gaps between states.[30] A purely *ab initio* 2005 study of the same three states by Tarczay *et al.* used single-reference coupled-cluster calculations with CBS extrapolation, and added significant corrections for core-correlation, relativistic effects and ZPE (using a quartic force-field).[33] The singlet-triplet gap predicted by Tarczay *et al.* (2170 ± 40 cm^{-1}) is in excellent agreement with experiment (2163.28 cm^{-1}). Our result of 2205 cm^{-1} (see Table IV) obtained using the multistate, multireference calculations described above is also in close agreement with experiment. The anharmonic corrections reported by Tarczay *et al.* for S_0 and S_1 are negligible (1-2 cm^{-1}) and despite the different approach, our optimized geometries and harmonic frequencies are extremely similar to theirs, and in good agreement with experiment (Table III).

TABLE III. Calculated geometric parameters (Å, degrees) and harmonic frequencies (cm^{-1}) for the S_0, S_1, S_2, and T_1 states of H(D)CCl at the MRCI(+Q)/CBS level (see text).

State	r_{CH}	r_{CCl}	Θ_{HCCl}	ω_1	ω_2	ω_3
S_0	1.1077	1.6915	102.45	2928.2 (2151.5)	1222.5 (908.2)	822.4 (811.5)
S_1	1.0837	1.6254	131.31	3165.3 (2335.1)	889.5 (672.4)	941.3 (923.9)
S_2	1.0661	1.5846	166.26	3400.5 (2524.8)	...[a]	1042.9 (1005.3)
T_1	1.0815	1.6550	126.52	3201.3 (2357.3)	897.8 (714.3)	961.2 (895.2)

[a]Bend levels were calculated using 1D DVR.

In Table IV we tabulate the calculated gaps between states and the extrapolation behavior of the various relative contributions. The reference energy (GDW-SA-CASSCF) makes up a large fractional contribution to the gaps from S_0 to S_1 and S_2, but a smaller fraction of the singlet-triplet gap. The reference energy converges rapidly (optimized power-law exponents are ~5.8–5.9) and values from the largest basis set are near the CBS limit. On the other hand, the all-electron correlation energy converges more slowly (optimized power-law exponents are ~2.35) than the l^{-3} rate commonly expected for valence-only correlation. The contribution to relative energies from the MRCI singles and doubles correlation is quite large for the gaps to S_1 and S_2, and is actually the largest component of the singlet triplet gap. Given its slow convergence, extrapolation of the correlation energy is a significant source of error. The recent development of multireference explicitly correlated F12 methods (MRCI-F12)[34] is very promising for improving the accuracy of this contribution. It is of concern when attempting to achieve chemical (or even spectroscopic) accuracy with multireference methods that the Davidson correction (+Q) to promote size extensivity can be quite large. For CHCl the contribution of the extrapolated Davidson correction (optimized power-law exponent ~3.45) to the gaps between S_0 and S_1 or T_1 is more than 1 kcal/mol, and is more than 3 kcal/mol for the gap to S_2. At this time it is far from routine to include higher order contributions to correlation for multireference methods.[35] Nevertheless, as shown in Table IV the calculated state origins are in relatively good agreement with experiment.

TABLE IV. Components of energy gaps between the S_0, S_1, S_2, and T_1 states of CHCl and their extrapolation behavior.

State	Ref. energy[a]	CBS exponent
S_0	0.0	5.808
S_1	14554.3	5.852
S_2	28302.7	5.897
T_1	428.2	5.776
State	Corr. energy[b]	CBS exponent
S_0	0.0	2.354
S_1	–1687.0	2.353
S_2	–5218.6	2.352
T_1	1212.0	2.352
State	(+Q) energy[c]	CBS exponent
S_0	0.0	3.465
S_1	–465.8	3.460
S_2	–1335.2	3.455
T_1	466.0	3.449
State	ΔZPE[d]	ΔSR corr.[e]
S_0	0.0	0.0
S_1	11.5	44.3
S_2	96.1[i]	68.1
T_1	43.6	55.0
State	Total energy[f]	Expt.
S_0	0.0	0.0
S_1	12457.3	12280[g]
S_2	21845.0	21491[h]
T_1	2204.8	2163.28

[a]Relative energies (cm^{-1}) for GDW-SA-CASSCF reference from aug-cc-pwCVnZ ($n = 3$–5) bases extrapolated with optimized power-law (see text).
[b]Correlation energy from similarly extrapolated MRCI calculations.
[c]Contribution from extrapolated Davidson-correction (see text).
[d]Difference in harmonic zero-point energy (see Table III).
[e]Difference in extrapolated relativistic energies (8th-order DKH, see text).
[f]Sum of all contributions.
[g]Experimental value from Ref. 38.
[h]Based on calculated extrapolation of observed bend progression (this work).
[i]Bending contribution to ZPE from 1D DVR calculation (see text).

Figure 6 displays single point energies of several important stationary points on the CHCl Potential Energy Surface (PES) computed at the MRCI(+Q) level of theory and, where possible, also at the single reference (R/U)CCSD(T) level. The valence correlated calculations were carried out using the aug-cc-pV(5+d)Z basis, i.e. with the inclusion of an extra set of tight 3d functions on Cl. Core-valence correlation corrections were obtained with cc-pwCVQZ basis, and scalar relativistic corrections, using the Douglas-Kroll approach, with the appropriate cc-pVQZ bases. The geometries and zero point energies were calculated at the CASPT2/cc-pV(T+d)Z level of theory. Our calculations show that the lowest energetic dissociation channel is to $C(^3P)$ + HCl, which occurs over a small barrier of ~6 kcal/mol, with a predicted energetic threshold of 71.9 kcal/mol (~25 150 cm^{-1}). Unlike the case of CHF, the S_2 origin in CHCl lies significantly below this barrier, and thus the lowest vibrational levels in S_2 are stable with respect to dissociation.

At higher energies, the MRCI calculations find the asymptotic thresholds (D_e) for C–H and C–Cl bond fission, with concomitant production of the CCl or CH radical in the ground $^2\Pi$ state, to lie at 77.6 kcal/mol (~27 140 cm^{-1}) and 88.7 kcal/mol (~31 020 cm^{-1}), respectively. We emphasize that the S_2 state does not adiabatically correlate with the $CCl(^2\Pi)$ + H asymptote, and thus the observed threshold, like that for S_1,[36] is probably higher. The threshold for the $C(^1D)$ + HCl channel lies much higher in energy, with the elimination occurring over a sizeable barrier, and is not important for the energy range probed here.

As the above results indicate, the coupled cluster method predicts a stronger C−Cl bond than the MRCI(+Q) approach. For example, the dissociation energy of the CHCl from its

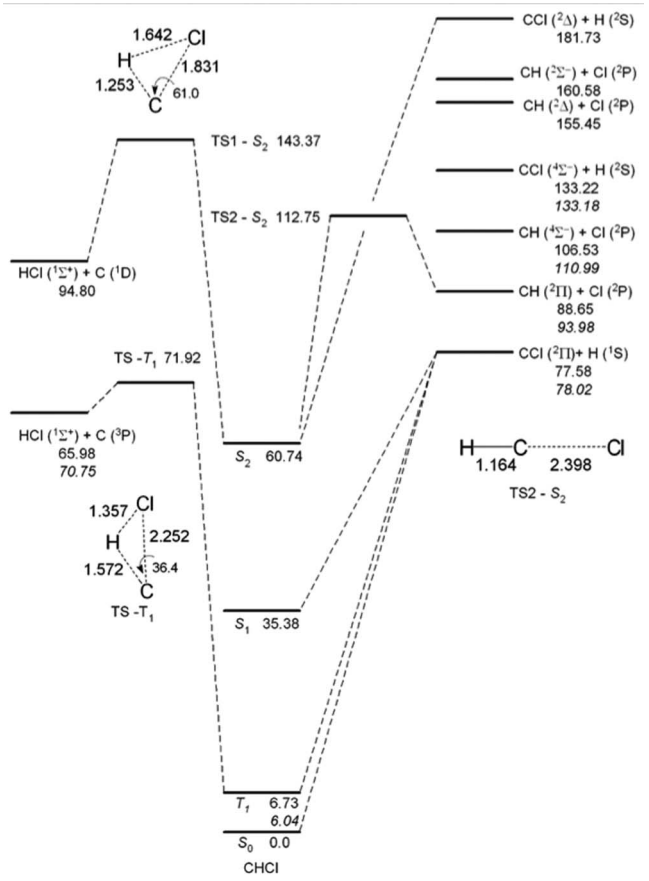

FIG. 6. Single point energies (in kcal mol^{-1}) of important stationary points on the CHCl potential energy surfaces, computed at MRCI(+Q) level of theory, as discussed in the text, and equilibrium geometries of the transition states. The figures in italics are the (R/U)CCSD(T) energies. Bond lengths are in Å and bond angles are in degrees.

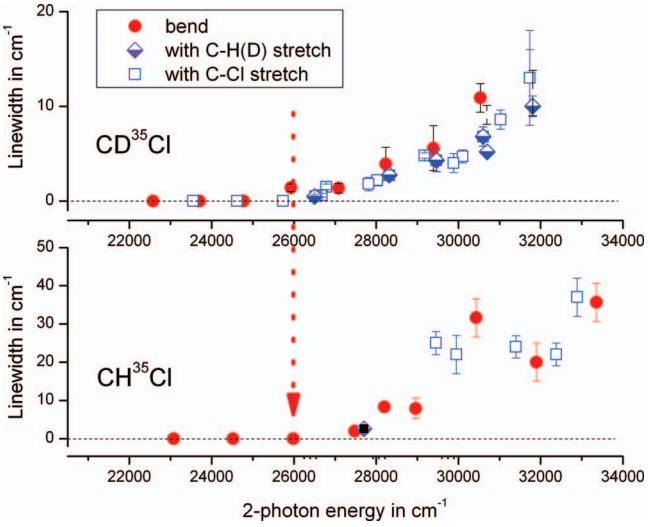

FIG. 7. Measured homogeneous linewidths in the S_2 states of $CD^{35}Cl$ (upper panel) and $CD^{35}Cl$ plotted as a function of energy above the vibrationless level of S_0.

ground state to CCl($^2\Pi$) + H is predicted to be 5.3 kcal mol^{-1} higher when computed at the (R/U)CCSD(T) level of theory. In light of the demonstrated accuracy of the CCSD(T) method for the prediction of accurate atomization energies of a range of halogenated compounds,[37] we regard the coupled cluster results as the more accurate, although in the context of this work the deficiencies of the MRCI(+Q) method are certainly not critical.

Figure 7 displays graphs of the measured linewidths in the S_2 state of $CH^{35}Cl$ and $CD^{35}Cl$; the values and associated uncertainties are listed in Table I. The data were plotted by grouping all levels in the (0, n^ℓ, 0), (0, n^ℓ, m), and (1, n^ℓ, m) progressions, in order to test for mode-specific effects like those present in the S_2 state of CHF,[8] where bending levels dissociate more rapidly, due to crossings with the S_3 state. The data shown in Fig. 7 reveal several important trends. First, for both $CH^{35}Cl$ and $CD^{35}Cl$ a clear onset of lifetime broadening is observed at between 26 000 and 27 000 cm^{-1} above the vibrationless level of S_0. A spectrum of a level in this region, the (0, 7^1, 2) level of $CD^{35}Cl$, is shown in Figure S4 in the supplementary material. Second, above this energy the linewidths appear to somewhat smoothly increase up to the maximum observed energy. Third, the linewidths for $CH^{35}Cl$ are consistently around two times larger than those for $CD^{35}Cl$; this trend is qualitatively similar to that observed in CHF. Finally, there is no discernable mode-specificity in the linewidths.

Our spectroscopic studies can only reveal the presence of lifetime broadening, without distinguishing the mechanism. The observed threshold (Fig. 7) lies roughly between the calculated barrier to HCl elimination on the triplet surface and the calculated threshold of the CCl($^2\Pi$) + H channel (Fig. 6), which we presume involves a modest exit channel barrier.[1] Although elimination to HCl would occur on the triplet surface, our Stimulated Emission Pumping study of S_0-T_1 coupling revealed a sizeable electronic spin-orbit matrix element of ~150 cm^{-1},[4] in good agreement with *ab initio* (MRCI) calculations at the seam of intersection.[30] If the observed threshold was due to the triplet channel, at higher energies a step in the linewidth coincident with the opening of the radical (bond-cleavage) channel should be observed; however, the increase in linewidth with energy remains monotonic. This may suggest that the experimental threshold represents that for C–H bond cleavage, CCl($^2\Pi$) + H, which is consistent with the reduced linewidths (lifetimes) for the deuterated isotopomer. Further experimental and theoretical studies will be needed to confirm this.

IV. CONCLUSIONS

We have reported the first observation of the quasi-linear, predissociated S_2 state of the monohalocarbene CHCl, using a fluorescence dip detected optical-optical double resonance strategy. Due to the pronounced Renner-Teller effect in the S_1 state, only intermediate levels of $K_a = 0$ were accessible, which restricted the observable levels in the S_2 state to those possessing vibrational angular momentum $l = 1$. Despite this limitation, we successfully observed a variety of S_2 bending vibrational levels in $CH^{35}Cl$ and its deuterated isotopomer, both alone and in combination with C–Cl and C–H stretch. The extrapolation of the experimental levels using the

bending levels derived from a 1-D calculation placed the origin of the S_2 state at 21 491 cm^{-1} above the ground state, compared with a calculated origin of 21 845 cm^{-1}.

The origin and low-lying vibrational levels of the S_2 state lie below the energetic threshold to dissociation via simple bond fission or elimination. At higher energies, clear line broadening is observed which, by analogy with CHF, is attributed to predissociation. The energetic onset of this broadening occurs between 26 000 and 27 000 cm^{-1} above the S_0 origin, and lies approximately in between the calculated thresholds for HCl elimination on the triplet surface, which is the lowest energy channel, and C–H bond fission. Future work will be needed to identify the products of the dissociation.

ACKNOWLEDGMENTS

S.A.R. acknowledges the National Science Foundation (Grants CHE-0717960 and CHE-1010597) for support of this research. R.D. acknowledges support by the University of Missouri Research Board. G.B.B. acknowledges the computing grants from the NCI-NF and Intersect Australia Ltd., and S.H.K. acknowledges the Australian Research Council (Grant DP0985767).

[1] S. H. Kable, S. A. Reid, and T. J. Sears, Int. Rev. Phys. Chem. **28**, 435 (2009).
[2] *Reactive Intermediate Chemistry*, edited by R. A. Moss, M. S. Platz, and M. Jones, Jr. (Wiley-Interscience, Hoboken, NJ, 2004).
[3] C. Tao, C. Mukarakate, R. H. Judge, and S. A. Reid, J. Chem. Phys. **128**, 171101/4 (2008).
[4] C. Tao, C. Mukarakate, Z. Terranova, C. Ebban, R. H. Judge, and S. A. Reid, J. Chem. Phys. **129**, 104309/8 (2008).
[5] G. Herzberg and J. W. C. Johns, Proc. R. Soc. London, Ser. A **295**, 107 (1966).
[6] Y. Kim, G. E. Hall, and T. J. Sears, J. Mol. Spectrosc. **240**, 269 (2006).
[7] Z. Wang, Y. Kim, G. E. Hall, and T. J. Sears, J. Phys. Chem. A **112**, 9248 (2008).
[8] C. Tao, S. A. Reid, T. W. Schmidt, and S. H. Kable, J. Chem. Phys. **126**, 051105/4 (2007).
[9] C. Richmond, C. Tao, C. Mukarakate, R. Dawes, E. C. Brown, S. H. Kable, and S. A. Reid, J. Chem. Phys. **135**, 104316 (2011).
[10] C. Tao, C. Richmond, C. Mukarakate, R. Dawes, S. H. Kable, and S. A. Reid, J. Chem. Phys. **135**, 104315 (2011).
[11] S. K. Shin and P. J. Dagdigian, J. Chem. Phys. **125**, 133317/1 (2006).
[12] S. K. Shin and P. J. Dagdigian, Phys. Chem. Chem. Phys. **8**, 3446 (2006).
[13] S. K. Shin and P. J. Dagdigian, J. Chem. Phys. **126**, 134302/1 (2007).
[14] S. K. Shin and P. J. Dagdigian, J. Chem. Phys. **128**, 154322/1 (2008).
[15] S. K. Shin and P. J. Dagdigian, J. Chem. Phys. **128**, 064309/1 (2008).
[16] M. R. Scholefield, S. Goyal, J. H. Choi, and H. Reisler, J. Phys. Chem. **99**, 14605 (1995).
[17] J. H. Choi, M. R. Scholefield, D. Kolosov, and H. Reisler, J. Phys. Chem. A **101**, 5846 (1997).
[18] D. C. Scott, J. Dejuan, D. C. Robie, D. Schwartzlavi, and H. Reisler, J. Phys. Chem. **96**, 2509 (1992).
[19] R. Guadagnini and G. C. Schatz, J. Phys. Chem. **100**, 18944 (1996).
[20] C. Mukarakate, C. Tao, C. D. Jordan, W. F. Polik, and S. A. Reid, J. Phys. Chem. A **112**, 466 (2008).
[21] C. Tao, C. Mukarakate, and S. A. Reid, J. Chem. Phys. **124**, 224314/11 (2006).
[22] C. Tao, C. Mukarakate, and S. A. Reid, J. Mol. Spectrosc. **241**, 143 (2007).
[23] R. Dawes, A. W. Jasper, C. Tao, C. A. Richmond, C. Mukarakate, S. H. Kable, and S. A. Reid, J. Phys. Chem. Lett. **1**, 641 (2010).
[24] H.-J. Werner, P. J. Knowles, F. R. Manby, and M. Schultz, MOLPRO, version 2010.1, a package of *ab initio* programs, 2010, see http://www.molpro.net.
[25] See supplementary material at http://dx.doi.org/10.1063/1.4748972 for three figures of additional data concerning the chlorocarbene potential energy surfaces.
[26] T. Helgaker, P. Jorgensen, and J. Olsen, *Molecular Electronic Structure Theory* (Wiley, New York, 2000).
[27] J. G. Hill, K. A. Peterson, G. Knizia, and H. J. Werner, J. Chem. Phys. **131**, 194105 (2009).
[28] A. Lin, K. Kobayashi, H.-G. Yu, G. E. Hall, J. T. Muckerman, T. J. Sears, and A. J. Merer, J. Mol. Spectrosc. **214**, 216 (2002).
[29] H.-G. Yu, J. T. Muckerman, and T. J. Sears, J. Chem. Phys. **116**, 1435 (2002).
[30] H.-G. Yu, T. J. Sears, and J. T. Muckerman, Mol. Phys. **104**, 47 (2006).
[31] A. J. Merer and D. N. Travis, Can. J. Phys. **44**, 525 (1966).
[32] G. Herzberg, *Molecular Spectra and Molecular Structure III. Electronic Spectra and Electronic Structure of Polyatomic Molecules* (Van Nostrand-Reinhold, New York, 1966).
[33] G. Tarczay, T. A. Miller, G. Czako, and A. G. Csaszar, Phys. Chem. Chem. Phys. **7**, 2881 (2005).
[34] T. Shiozaki, G. Knizia, and H. J. Werner, J. Chem. Phys. **134**, 034113 (2011).
[35] P. G. Szalay, T. Muller, G. Gidofalvi, H. Lischka, and R. Shepard, Chem. Rev. **112**, 108 (2012).
[36] K. Sendt, T. W. Schmidt, and G. B. Bacskay, Int. J. Quant. Chem. **76**, 297 (2000).
[37] D. Feller, K. A. Peterson, W. A. de Jong, and D. A. Dixon, J. Chem. Phys. **118**, 3510 (2003).
[38] B.-C. Chang and T. J. Sears, J. Chem. Phys. **102**, 6347 (1995).